Hydration and Counterion Binding of [C_{12}MIM] Micelles

Sergej Friesen,[†] Thomas Buchecker,[‡] Alice Cognigni,[¶] Katharina Bica,[¶] and Richard Buchner*[,†]

Institut für Physikalische und Theoretische Chemie, Universität Regensburg, Regensburg, Germany, Institut für Anorganische Chemie, Universität Regensburg, Regensburg, Germany, and Institut für Angewandte Synthesechemie, Technische Universität Wien, Vienna, Austria

E-mail: richard.buchner@chemie.uni-regensburg.de

Abstract

Surface-active ionic liquids based on imidazolium cations are promising targets for micellar catalysis in aqueous solution, yielding enhanced rate constants compared to surfactants based on *n*−alkyltrimethylammonium cations and exhibiting a pronounced counterion dependence.[1,2] Probably most relevant to that is the interplay of headgroup hydration and counterion binding. To get more detailed information on these effects aqueous solutions of 1-dodecyl-3-methylimidazolium ([C_{12}MIM]) bromide, iodide and triflate (TfO^-) were investigated at 45 °C using broadband dielectric spectroscopy, viscosity measurements and small-angle X-ray scattering experiments. Effective hydration numbers were determined and information on the location and mobility of the condensed counterions, X^-, was derived. It turned out that [C_{12}MIM]-halide micelles

*To whom correspondence should be addressed
[†]Institut für Physikalische und Theoretische Chemie, Universität Regensburg, Regensburg, Germany
[‡]Institut für Anorganische Chemie, Universität Regensburg, Regensburg, Germany
[¶]Institut für Angewandte Synthesechemie, Technische Universität Wien, Vienna, Austria

were less hydrated than corresponding *n*-dodecyl-trimethylammonium ([C_{12}TA]X) aggregates. Together with their somewhat weaker counterion condensation this probably explains their higher catalytic activity. Whilst [C_{12}MIM]Br micelles remained roughly spherical in the studied concentration range, rod-like aggregates were formed at high concentrations of the iodide and in particular the triflate surfactant. It appears that the much lower mobility of condensed TfO^- counterions is the reason for the very low catalytic activity of [C_{12}MIM]TfO micelles.

Introduction

Since the discovery of ionic liquids (ILs) by Paul Walden in 1914,[3] these compounds continue attracting the attention of chemists around the world. Defined as salts melting below 100 °C,[4] their unique physico-chemical properties, such as negligible vapor pressure, high thermal and chemical stability, low flammability and high charge density,[5,6] have aroused increasing industrial and fundamental interest. Possible applications of ILs range from their use as alternative solvents in extraction/separation, electrochemical and catalytical processes to materials engineering.[5,7] Research into that direction is mainly focused on pure ILs or on situations where these compounds are a major mixture component but also dilute IL solutions are gaining increasing interest.[8–10]

Due to their structure, consisting of a hydrophobic residue —often an alkyl chain— attached to a charged moiety, many ions used as building blocks of ILs are amphiphilic and thus prone to self-association,[11] including the formation of micelles in dilute aqueous solution.[9,12] Typical examples of such surface-active ionic liquids (SAILs), which form micelles for $n \geq 8$, are 1-alkyl-3-methylimidazolium ILs, [C_nMIM]X, where X is the anion and n the number of carbon atoms in the alkyl chain.[13–16] In that respect but also from a structural point of view they resemble *n*-alkyl-trimethylammonium salts, [C_nTA]X, a classical family of cationic surfactants[17] serving here as a convenient reference.

Recent studies revealed the outstanding performance of [C_{12}MIM]X SAILs in mi-

cellar extraction processes[18,19] and for the micellar catalysis of Diels Alder reactions,[1] oxidations[20–22] and nucleophilic substitution (S_N) reactions.[2] In the latter case, a marked influence of the anion on the reaction rate constant, k, of a model S_N reaction was observed, with $k(Cl^-) > k(Br^-) > k(I^-) > k(TfO^-)$ (TfO^- - triflate, trifluoromethanesulfonate). For charged micelles to be stable counterions have to condense on their surface, reducing thus Coulomb repulsion between the surfactant headgroups.[23] Therefore, it is reasonable to assume that the anion effect observed for k is related to the extent and also the strength of counterion binding on the micellar surface. For the latter not only the Coulomb interactions between the anions and the cationic surfactant headgroups are relevant but also the hydration of both.

Broadband dielectric relaxation spectroscopy (DRS) probes the interaction of the sample with a small-amplitude electromagnetic field and thus provides information on the structure and collective dynamics of the studied system.[24] This technique has proven to be a very useful tool for the investigation of solute-solute, solute-solvent and solvent-solvent interactions in systems ranging from pure dipolar fluids[25] to electrolyte solutions.[26,27] In the case of ionic surfactant systems DRS allows the determination of effective hydration numbers and —via micelle-specific modes— yields insights into the location and mobility of condensed couterions.[28–33] Accordingly, we present in this contribution a dielectric study of aqueous solutions of the SAILs 1-dodecyl-3-methylimidazolium bromide ($[C_{12}MIM]Br$), 1-dodecyl-3-methylimidazolium iodide ($[C_{12}MIM]I$) and 1-dodecyl-3-methylimidazolium trifluoromethanesulfonate ($[C_{12}MIM]TfO$) at 45 °C to elucidate the impact of different counterions on the dynamics and hydration of the formed micelles. Measurements covered the concentration range $cmc < c < 250$ mM (*i.e.* 10^{-3} mol/L) where *cmc* is critical micellar concentration (Table 1). The triflate counterion was chosen as it exhibited the lowest reaction rate constant in the investigation of Cognigni *et al.*[2] on micellar catalysis. Although the Br^- ion yielded only the second fastest rate in the latter study, it was preferred over Cl^- for the present investigation as dielectric data for dodecyl-trimethylammonium

bromide ([C_{12}TA]Br) were available for comparison.[28,29,32] The rate constant for I^- was intermediate to those of Br^- and TfO^-. Additionally, dielectric measurements of selected samples were performed in the temperature range of (25 to 65) °C to determine Eyring activation enthalpies and entropies of the observed relaxation processes.[34] These investigations were complemented by viscosity measurements and small-and-wide-angle X-ray scattering (SWAXS) experiments to gain further information on the aggregation behavior.

Experimental

Materials. Except for 1-bromdodecane, which was distilled at 170 °C under reduced pressure (55 mbar), all chemicals required for the synthesis of the surfactants were used as received. The halide-based imidazolium ILs were synthesized by reacting 1-methylimidazole (Carl Roth, ≥ 99%) with a slight molar excess (1.2 equivalents) of the appropriate 1-halododecane (Sigma-Aldrich, > 97%).[35] After the reaction [C_{12}MIM]Br was recrystallized three times from ethyl acetate (Acros Organics, 99.97%), whereas toluene (VWR Chemicals, ≥ 99.5%) was used to recrystallize [C_{12}MIM]I thrice. The latter compound was subsequently washed three times with *n*-hexane (VWR Chemicals, 99%). In both cases colorless crystalline solids were obtained which were then dried at room temperature under reduced pressure ($p \leq 2 \cdot 10^{-6}$ bar) over P_2O_5 (Siccapent, Merck) as a desiccant for four days. The water content determined by Karl Fischer titration was found to be < 370 ppm for [C_{12}MIM]Br and < 70 ppm for [C_{12}MIM]I.

[C_{12}MIM]TfO was prepared according to ref. 2. The required chemicals methyl triflouromethane sulfonate and dichlormethane were acquired from Carbolution Chemicals (97 %) and Acros Organics (> 99.8%) respectively. *N*-dodecylimidazole was synthesized as described by Souza *et al.*[36] and subsequently distilled at 140 °C under $3 \cdot 10^{-5}$ bar. The freshly synthesized [C_{12}MIM]TfO was washed four times with *n*-hexane (VWR Chemicals, 99%) to give a colorless solid which was subsequently dried under high vacuum

($p \leq 10^{-8}$ bar) at 45 °C for four days. The water content of the final product was < 260 ppm.

For all synthesized ILs purity was checked by ^{1}H-NMR, ^{13}C-NMR and elemental analysis. The water used for sample preparation was purified with a Millipore Q-MILLI purification unit and showed a specific electrical resistance of ≥ 18 MΩcm. Aqueous $[C_{12}MIM]X$ solutions of solute molality, m (in mol·kg^{-1} solvent), were prepared gravimetrically without buoyancy correction.

Auxiliary Measurements. To obtain the molar solute concentration, c (in mol·L^{-1} = M), of the sample of molality m solution densities, ρ, were determined with an Anton Paar DMA 5000 vibrating tube densimeter having $5 \cdot 10^{-6}$ g·cm^{-3} nominal uncertainty and 0.005 K temperature stability. Viscosities, η, of the micellar solutions were obtained with an Anton Paar AMVn rolling ball viscometer having an uncertainty of 0.05 K in temperature, T, and a relative uncertainty of 0.02 in η. The electrical conductivity, κ, of the samples used for DRS was determined with the equipment described previously, having a temperature uncertainty of 0.005 K and a relative uncertainty in κ of 0.015.[37] The thus obtained data for ρ, η and κ are summarized in Tables S1-S6 of the Supporting Information.

Additionally, the critical micellar concentration, *cmc*, of the three surfactants in water at (45.0 ± 0.1) °C was determined by conductivity measurements with a WTW inoLab Cond 730 conductivity meter. The *cmc* was obtained from the intersection of the two straight lines observed for $\kappa(c)$ at $c < cmc$ and $c > cmc$ respectively (Figure S1 of the Supporting Information). The obtained *cmc* values and the degree of counterion binding, β, estimated from the ratio of the slopes above and below *cmc*,[38] are presented in Table 1. As expected for ionic surfactants,[23] the *cmc* decreased with increasing β, *i.e.* decreasing headgroup repulsion, yielding the anion sequence $Br^- > I^- > TfO^-$. The obtained data for *cmc* and β compare reasonably with literature values for 25 °C, except for the rather small β value published for $[C_{12}MIM]TfO$ (Table 1).[1]

Small-and-wide angle X-ray Scattering. Small-and-wide-angle X-ray scattering (SWAXS) is one of the most established methods to examine the mesoscale structure of soft matter.

The instrumentation used for the present SWAXS measurements was described in details elsewhere.[39] The scattered intensities were recorded as a function of the magnitude of the scattering vector, $q = [(4\pi)/\lambda] \times \sin(\theta/2)$, where λ is the wavelength of incident radiation and θ the scattering angle. Quartz capillaries of 2 mm diameter were used as sample containers. The usual corrections for the background (empty cell and detector noise) and an intensity normalization, using a high-density polyethylene film as a standard, were applied. Silver behenate in a sealed capillary was used to calibrate the scattering vector. The experimental resolution was $\Delta q/q = 0.05$. All measurements were performed at room temperature. The FIT2D software[40] was used for data analysis.

Table 1: Critical micelle concentrations, *cmc*, and degrees of counterion binding, β, of the investigated SAILs at 45 °C in comparison with literature data.

	45 °C		25 °C	
SAIL	*cmc* / mM	β	*cmc* / mM	β
$[C_{12}MIM]Br$	10.03	0.64	10.29[a]	0.70[a], 0.75[b]
$[C_{12}MIM]I$	7.13	0.78	5.19[a]	0.84[a], 0.85[b]
$[C_{12}MIM]TfO$	3.58	0.80	3.31[a]	0.73[a]

[a] taken from Ref. 2; [b] taken from Ref. 41.

Dielectric Relaxation Spectroscopy. DRS probes the macroscopic polarization of a sample induced by an applied electric field of frequency ν.[24] This response is conveniently expressed in terms of the generalized complex permittivity[42]

$$\hat{\eta}(\nu) = \hat{\varepsilon}(\nu) - \frac{i\kappa}{2\pi\nu\varepsilon_0} = \varepsilon'(\nu) - i[\varepsilon''(\nu) + \frac{\kappa}{2\pi\nu\varepsilon_0}] \quad (1)$$

In eq 1, $\varepsilon'(\nu)$ is the relative permittivity of the sample and $\varepsilon''(\nu)$ the associated dielectric loss; ε_0 denotes the permittivity of vacuum. The last term in the equation describes energy dissipation arising from the dc ($\nu = 0$) conductivity, κ, of the sample whereas the complex permittivity, $\hat{\varepsilon}(\nu) = \varepsilon'(\nu) - i\varepsilon''(\nu)$, comprises all contributions that explicitly depend on

frequency and thus provides information on the cooperative dynamics of the investigated system.

The generalized permittivity was recorded in the frequency range of $0.02 \leq \nu/\mathrm{GHz} \leq 89$. For $\nu \leq 50$ GHz a frequency-domain reflectometer was used. This setup is based on an Agilent E8364B vector network analyzer (VNA) in combination with two open-ended coaxial dielectric probes, Agilent 85070E-20 (0.2-20 GHz) and 85070-50 (5-50 GHz),[43] and a coaxial cut-off cell for 0.02-1 GHz. For $60 \leq \nu/\mathrm{GHz} \leq 89$ a waveguide interferometer with variable-pathlength transmission cell was used. For all three surfactants $\hat{\varepsilon}(\nu)$ was recorded as a function of solute concentration in the range $cmc \lesssim c \lesssim 260$ mM at the temperature of 318.15 K. Additionally, for each SAIL one of these solutions ([C_{12}MIM]Br: 0.1033 mol·kg^{-1}, corresponding to c = 99.2 mM at 318.15 K; [C_{12}MIM]I: 0.1038 mol·kg^{-1}/99.5 mM at 318.15 K; [C_{12}MIM]TfO: 0.0749 mol·kg^{-1}/74.4 mM at 318.15 K) was studied as a function of temperature for $298.15 \leq T/\mathrm{K} \leq 338.15$. The temperature uncertainty of the dielectric experiments was 0.05 K.

After concatenating the data obtained with the different instruments $\hat{\eta}(\nu)$ was corrected for dc conductivity to yield $\varepsilon''(\nu)$. Where required, $\varepsilon'(\nu)$ was additionally corrected for electrode polarization as described in ref. 24 (Fig. S2). For the thus obtained dielectric spectra, $\hat{\varepsilon}(\nu)$, the associated relaxation-time distribution function, $P(\tau)$, was determined using Zasetzky's method[44] to restrict the number of relaxation models to be tested in subsequent fits of $\hat{\varepsilon}(\nu)$ with sums of n Havriliak-Negami equations.[26] At $c > cmc$ the obtained $P(\tau)$ spectra, Figs. S3–S8, suggest the presence of four relaxations centered at approximately 5 ps (corresponding to ~30 GHz), 100 ps (1.5 GHz), 400 ps (0.4 GHz) and 1-3 ns (0.09-0.16 GHz) for all studied solutions. Subsequent testing of all possible models with $2 \leq n \leq 5$ assumed modes along the criteria described in detail previously[25] revealed that these spectra could be consistently fitted with a superposition of four Debye equations

$$\hat{\varepsilon}(\nu) = \sum_{j=1}^{4} \frac{S_j}{1 + \mathrm{i}2\pi\nu\tau_j} + \varepsilon_\infty \qquad (2)$$

In this D+D+D+D model S_j is the amplitude and τ_j the relaxation time of the modes $j = 1 \ldots 4$ resolved at increasing frequencies; $\varepsilon_\infty = \lim_{\nu\to\infty} \varepsilon'(\nu)$ is the high-frequency permittivity. The static relative permittivity of the sample is given as $\varepsilon = \varepsilon_\infty + \sum S_j$. Examples of the dielectric spectra spectra and their fits are shown in Figs. 1-3. The obtained parameters are summarized in Tables S7–S12.

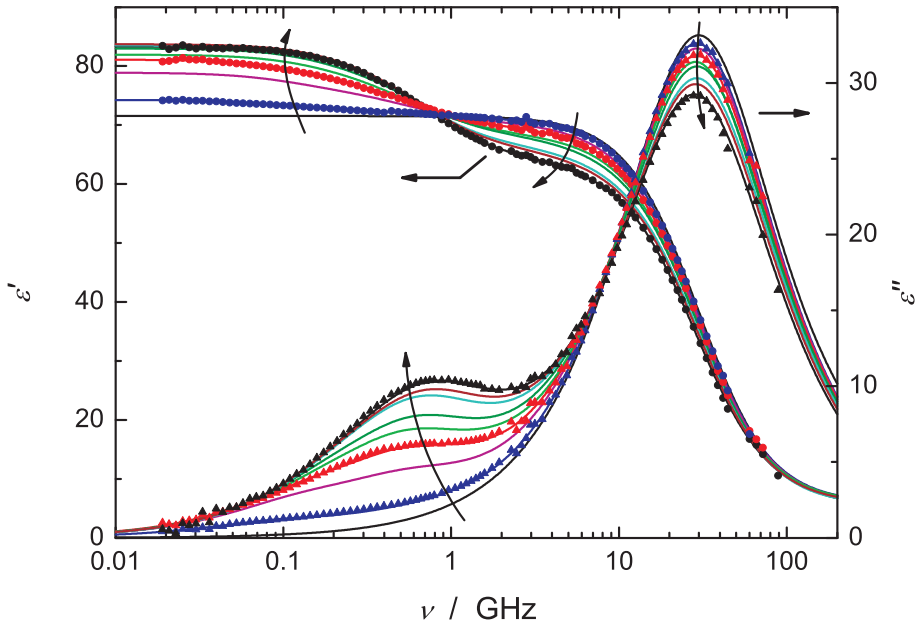

Figure 1: Spectra of relative permittivity, $\varepsilon'(\nu)$ (▲), and dielectric loss, $\varepsilon''(\nu)$ (●), and their fits with eq 2 (lines) of aqueous $[C_{12}MIM]Br$ solutions at 45 °C and concentrations c = (0, 19.9, 49.4, 74.7, 99.2, 125.0, 173.8, 199.6 and 242.1) mM in arrow direction. For clarity experimental data are only shown for selected samples.

For the three IL samples with $c \approx cmc$ mode $j = 3$ could not be resolved and also S_1 and S_2 are very small and biased. Accordingly, the parameters of the D+D+D fit to these spectra were not considered in the further analysis but their values are given in Tables S7–S9 for completeness. Note that for higher concentrations the D+D+CC model, *i.e.* two Debye functions for the micelle-specific modes and a symmetrically broadened Cole-Cole function for the solvent, produced fits of a quality similar to the D+D+D+D model. However, the derived hydration numbers were un-physical so that the D+D+CC model was discarded.

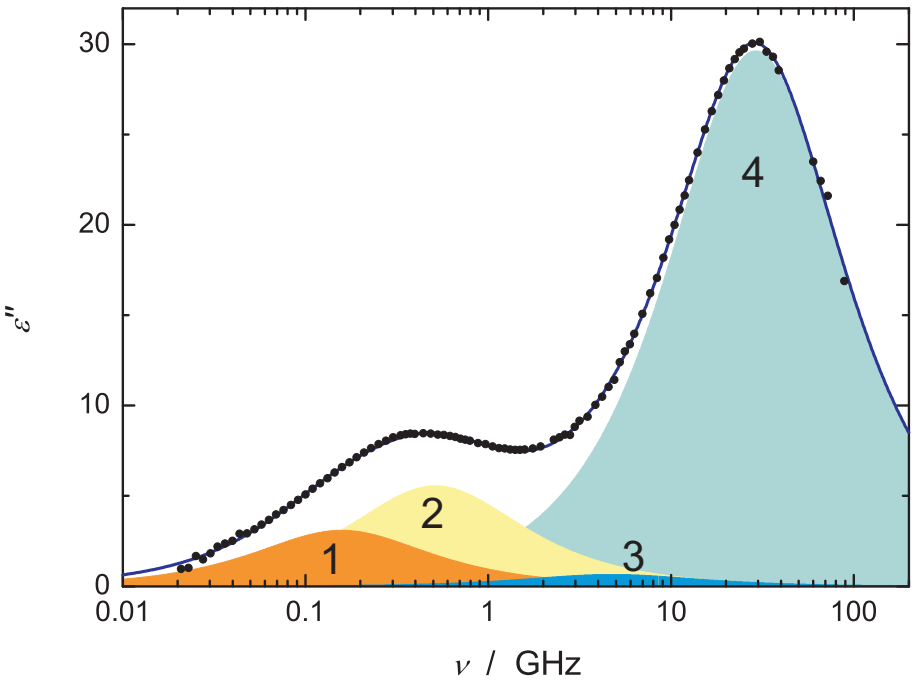

Figure 2: Dielectric loss, $\varepsilon''(\nu)$ (●), spectrum of 230.1 mM aqueous $[C_{12}MIM]I$ at 45 °C and associated fit with the D+D+D+D model (line). The shaded areas show the contributions of the resolved modes, $j = 1 \ldots 4$.

Results

Dielectric Spectroscopy

Assignment of Relaxation Modes. The dominating relaxation process at ~ 30 GHz ($\tau_3 \approx$ 5.4 ps) can be readily assigned to the cooperative (c) rearrangement of the H-bond network of bulk-like water as for pure H_2O at 45 °C the corresponding relaxation time is τ_c = 5.33 ps[45] and the present data for τ_3 smoothly evolve from that value (Tables S7–S9). Since the present spectra extend only to 89 GHz the fast (f) water mode (τ_f = 0.165 ps at $c = 0$) could not be resolved but its presence is obvious from the obtained high-frequency permittivity values ($\varepsilon_\infty(c) \approx 5$) which significantly exceed the pure-water value ($\varepsilon_\infty(0)$ = 2.78).

Upon surfactant addition a broad micelle-specific contribution appeared at $c > cmc$ in the 0.05 to 5 GHz region of the dielectric spectra (Fig. 1). This feature shifted to lower

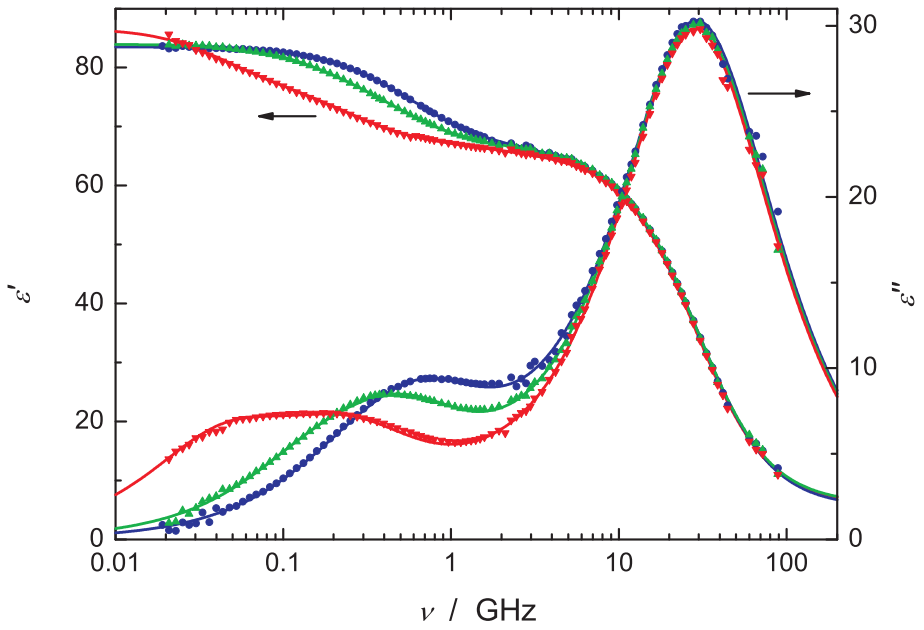

Figure 3: Dielectric loss, $\varepsilon''(\nu)$ (symbols), spectra and their fits with eq 2 (lines) of aqueous solutions of 173.8 mM $[C_{12}MIM]Br$ (●), 173.9 mM $[C_{12}MIM]I$ (▲) and 173.9 mM $[C_{12}MIM]TfO$ (▼) at 45 °C.

frequencies when going from Br^- to I^- to TfO^- (Fig. 3) and —as predicted by the theory of Grosse[46] for suspensions of charged colloids— was well described by two additional Debye relaxations (Fig. 2). Accordingly, we assigned the lowest-frequency mode centered at ~ 0.1 GHz to fluctuations of the diffuse counterion cloud surrounding the micelles, whereas the intermediate-frequency mode at ~0.4 GHz was attributed to the hopping of condensed counterions on the surface of the micelle.[29,31]

Only with the assumption of an additional weak mode, (S_3, τ_3), located between the micelle-specific relaxations and the dominating contribution from bulk-like water consistent sets of relaxation parameters as a function of concentration (Tables S7–S9) and temperature (Tables S10–S12) could be obtained. Due to its small amplitude, $S_3 < 3$, the obtained parameters were very noisy and in some cases τ_3 had to be fixed in the fit to get reasonable S_3 values. Despite the large variation of τ_3 with the anion and (partly) with c and T we assign this relaxation to retarded (slow) H_2O molecules hydrating the micelles for the reasons discussed below.

The contribution of free SAIL cations to the dielectric spectra could be neglected as their concentration is comparable to the *cmc* and thus very low.[47] Also the contribution of free triflate anions is negligible.[48]

Eyring Activation Parameters. The relaxation times, τ_j ($j = 1 \ldots 4$), of the solutions investigated as a function of temperature in the range $298.15 \leq T/\mathrm{K} \leq 338.15$ (Tables S10–S12) were fitted to the Eyring equation[34]

$$\ln(\tau_j/\mathrm{s}) = \ln\left(\frac{h}{k_\mathrm{B}T}\right) - \frac{\Delta S^{\neq}}{R} + \frac{\Delta H^{\neq}}{RT} \tag{3}$$

where the activation entropy, $\Delta S^{\neq}$, and the activation enthalpy, $\Delta H^{\neq}$, were assumed to be independent of T; h, k_b and R have their usual meaning. The obtained activation parameters are summarized in Table 2; corresponding fits are shown in Figs. S9-S11. The results for τ_3 have to be taken with a grain of salt as the amplitude of this mode is very small. Therefore, not only S_3 but also the corresponding relaxation time is very sensitive to experimental error. For some spectra values of τ_3 (open symbols in Figs. S10 & S11) even had to be fixed to get reasonable fits with eq 2, which obviously might bias $\Delta H^{\neq}$ and $\Delta S^{\neq}$.

In line with current understanding of water dynamics, which assumes jump reorientation via a triangular transition state,[50] not only the activation enthalpy for the cooperative water relaxation but also the corresponding entropy was found to be positive for the three investigated SAIL solutions. Within experimental uncertainty $\Delta S^{\neq}(\tau_4)$ and $\Delta H^{\neq}(\tau_4)$ are independent of the anion but both quantities are somewhat reduced compared to pure water.[51] Thus, all three solutes facilitate bulk-water reorientation to some extent. Almost certainly, this is mainly due to the labile hydration shells of the present anions, Br^-,[52] I^-,[50,52] and TfO^-,[53] which cannot be distinguished from bulk water by DRS.[26]

Activation enthalpy and entropy of the slow-water mode strongly depend on the anion. Both quantities decrease in the sequence $Br^- < I^- < TfO^-$. Although other possible sources for the pronounced change of τ_3 with temperature, in particular for Br^-, cannot be excluded

Table 2: Eyring activation enthalpy, $\Delta H^{\neq}$, and activation entropy, $\Delta S^{\neq}$, of relaxation times, $\tau_j(T)$ ($j = 1 \ldots 4$), of the solutions investigated as a function of T.

system	τ_j	$\Delta H^{\neq}$ / kJ mol^{-1}	$\Delta S^{\neq}$ / J mol^{-1}K^{-1}
water	τ_b [a]	15.9 ± 0.2	20.4 ± 0.7
[C_{12}MIM]Br	τ_1	20 ± 6	−8 ± 18
b = 0.1033 mol/kg	τ_2	20.6 ± 0.8	−2 ± 3
(99.2 mM at 45 °C)	τ_3	71 ± 10	174 ± 31
	τ_4	14.0 ± 0.4	14.1 ± 1.2
[C_{12}MIM]I	τ_1	10 ± 3	−44 ± 8
b = 0.1038 mol/kg	τ_2	13.7 ± 0.8	−20 ± 3
(99.5 mM at 45 °C)	τ_3	19.8 ± 1.4	17 ± 4
	τ_4	14.0 ± 0.5	14 ± 2
[C_{12}MIM]TfO	τ_1	15 ± 2	−38 ± 6
b = 0.0749 mol/kg	τ_2	15 ± 3	−21 ± 9
(74.4 mM at 45 °C)	τ_3	13 ± 3	−14 ± 10
	τ_4	13.6 ± 0.3	12.8 ± 1.1

[a] Ref. 49.

the data appear to be reasonable (see Discussion).

The activation parameters obtained for the two micelle-specific modes are not very reliable but trends can be noted from Table 2. For both relaxation times, τ_1 & τ_2, the sequence $I^- < TfO^- < Br^-$ was found for $\Delta H^{\neq}$. On the other hand for bromide $\Delta S^{\neq}$ is negligible for both micelle relaxations whereas for the other two anions the activation entropies are clearly negative and similar in magnitude, with $\Delta S^{\neq}(\tau_1) \approx 2\Delta S^{\neq}(\tau_2)$.

Water Relaxation and Hydration Numbers. The amplitudes, S_i, of relaxation processes associated with the reorientation of molecular dipoles can be analyzed with the equation

$$\frac{\varepsilon + A_i(1-\varepsilon)}{\varepsilon} S_i = \frac{N_A c_i}{3\varepsilon_0 k_B T} \cdot \mu_{\mathrm{eff},i}^2 \tag{4}$$

where c_i is the molar concentration of the involved species, i, $\mu_{\mathrm{eff},i}$ its effective dipole moment and A_i the associated cavity field factor; N_A is the Avogadro constant.[27] For

water molecules the assumption of a spherical cavity, $A = 1/3$, is reasonable and for the evaluation of solvent modes normalization to the pure state is convenient as it allows elimination of $\mu_{\mathrm{eff},i}$.

For water the fast jump reorientation of a molecule, probably associated with the fast relaxation (τ_f = 165 fs at 45 °C), and the subsequent settling of the H-bond network and waiting for the next jump, governed by τ_c = 5.33 ps, form a continuous sequence of events and accordingly the sum of both amplitudes, $S_b = S_c + S_f$, has to be evaluated with eq 4.[27] This is also the case for solution spectra. Since no fast water mode was resolved from the present solution spectra the amplitude of bulk water was approximated as $S_b(c) = S_4(c) + \varepsilon_\infty(c) - \varepsilon_\infty(0)$.

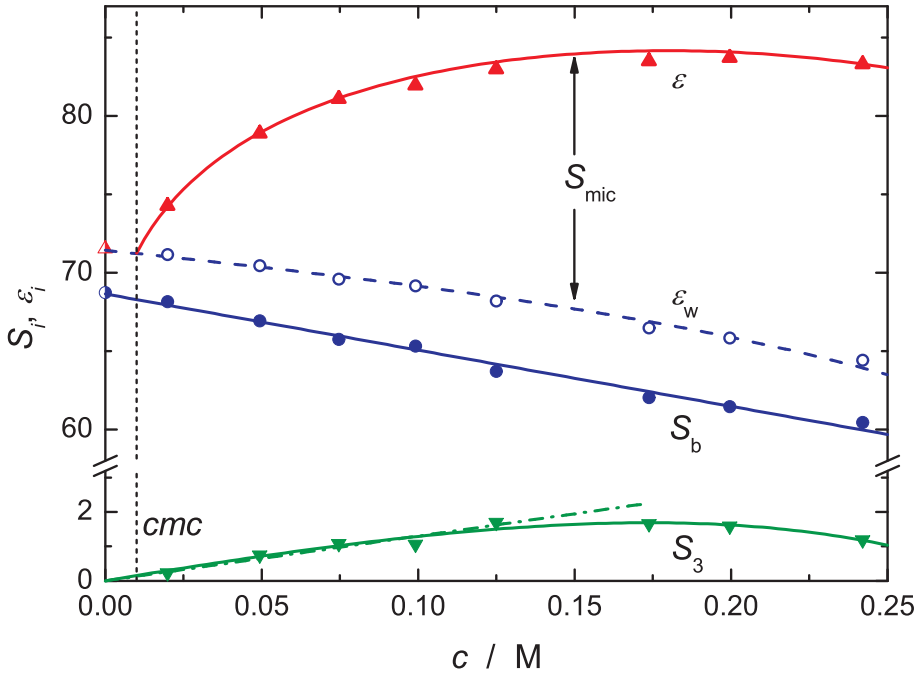

Figure 4: Static permittivity of the solution, ε (▲), and corresponding contribution of water, $\varepsilon_w = \varepsilon - S_1 - S_2$ (○), for aqueous [C_{12}MIM]Br solutions at 45 °C. Also shown are the corresponding amplitudes of bulk, S_b (●), and slow water, S_3 (▼). Lines are a guide to the eye, with the dash-dotted line highlighting the linear increase of S_3 at $c \leq 125$ mM and the vertical line indicating the *cmc*.

From S_b the concentration of bulk-like water, c_b, can be obtained whereas S_3 yields the concentration of moderately retarded (slow) solvent, c_s. These quantities then allow

calculating the total effective hydration number, $Z_t = (c_w - c_b)/c$ (c_w is the analytical solvent concentration), and the number of retarded H_2O molecules per equivalent of solute, $Z_s = c_s/c$.[26,27] The difference $Z_{ib} = Z_t - Z_s$ gives the number of water dipoles which are so strongly impeded (irrotationally bound, ib) in their rotation that they disappear from the spectrum.

A problem with the direct calculation of Z_t and Z_s is that with decreasing solute concentration their uncertainties strongly increase as the amplitude error remains constant whereas $(c_w - c_b)$ respectively c_s get smaller and smaller. However, for all three SAILs investigated S_b decreases linearly with solute concentration (Fig. 4). Additionally, S_3 increases linearly over the entire range investigated for $[C_{12}MIM]I$ and $[C_{12}MIM]TfO$. For $[C_{12}MIM]Br$ this is only true for $c \leq 125$ mM (Fig. 4). Since also solution density, ρ, and conductivity, κ, exhibit straight lines over the entire concentration range it is convenient to focus on the well-defined slopes of these quantities. To do so, eq 4 was rearranged to give the $c \to 0$ limit

$$Z_t^0 = \lim_{c\to 0}\left(\frac{dc_w}{dc}\right) - \lim_{c\to 0}\left(\frac{dc_b^{eq}}{dc}\right) \tag{5}$$

where

$$\lim_{c\to 0}\left(\frac{dc_w}{dc}\right) = \left[\lim_{c\to 0}\left(\frac{d\rho}{dc}\right) - M\right]/M_s \tag{6}$$

with M and M_s as the molar masses of solute and solvent, and

$$\lim_{c\to 0}\left(\frac{dc_b^{eq}}{dc}\right) = \frac{c_w(0)}{S_b(0)} \times \left[\lim_{c\to 0}\left(\frac{dS_b}{dc}\right) + \xi \times \lim_{c\to 0}\left(\frac{d\kappa}{dc}\right)\right] \tag{7}$$

In this approach the second summand in eq 7, with

$$\xi = p \times \frac{\varepsilon(0) - \varepsilon_\infty(0)}{\varepsilon(0)} \times \frac{\tau(0)}{\varepsilon_0} \tag{8}$$

corrects for kinetic depolarization assuming slip boundary conditions ($p = 2/3$) for ion transport.[54] Similarly, for linearly increasing S_3 the low-c limit of the slow-water solvation

number is given by

$$Z_s^0 = \lim_{c\to 0}\left(\frac{dc_s}{dc}\right) = \frac{c_w(0)}{S_b(0)} \times \lim_{c\to 0}\left(\frac{dS_3}{dc}\right) \quad (9)$$

Obviously, for $[C_{12}MIM]Br$ at $c > 125$ mM values for $Z_s(c)$ had to be calculated directly as described in detail in Ref. 27.

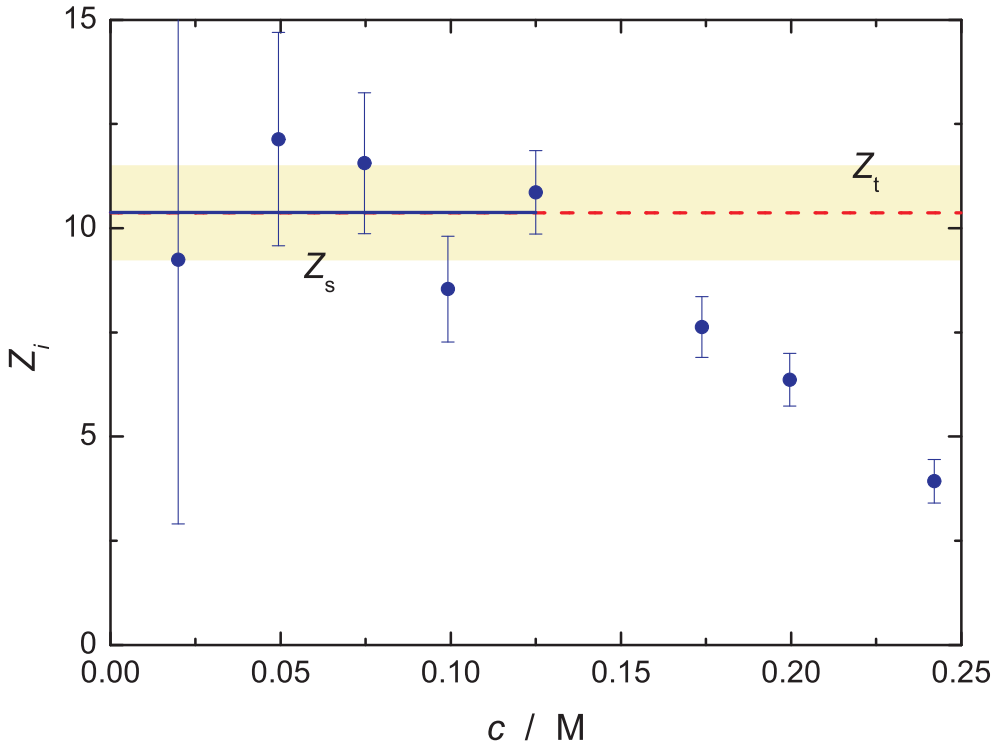

Figure 5: Total hydration number, Z_t (broken line), and associated standard uncertainty (shaded area) of $[C_{12}MIM]Br$ in aqueous solution at 45 °C. Also indicated is the corresponding number of slow (retarded) H_2O molecules per equivalent of solute, Z_s, obtained with eq 9 from the slope dS_3/dc for $c \le 125$ mM (solid line; on top of Z_t) and directly calculated values (●).

Table 3 summarizes the obtained Z_t^0 and Z_s^0 values. Figure 5 compares for $[C_{12}MIM]Br$ the result obtained with eq 9 for $c \le 125$ mM with directly calculated Z_s values for the entire concentration range. For $[C_{12}MIM]Br$ up to 125 mM and for all $[C_{12}MIM]TfO$ solutions $Z_t^0 = Z_s^0$ within experimental uncertainty. On the other hand, for $[C_{12}MIM]I$ $Z_{ib} \approx 6$ at all studied c and for $[C_{12}MIM]Br$ the number of strongly bound water molecules, $Z_{ib} = Z_t - Z_s$, increases from zero at $c \le 125$ mM to ~ 6 at 242 mM whilst the total hydration number

Table 3: Effective total hydration numbers, Z_t^0, and numbers of slow (moderately retarded) water, Z_s^0, of the investigated $[C_{12}MIM]X$ surfactants at 45 °C and of comparable $[C_{12}TA]X$ surfactants from the literature.

	$[C_{12}MIM]X$		$[C_{12}TA]X$	
X^-	Z_t^0	Z_s^0	Z_t^0	Z_s^0
Br^-	10.4 ± 1.4	10.4 ± 0.6	22 ± 3 [a]	12 ± 2 [a]
			21 ± 3 [b]	11 ± 2 [b]
I^-	11.8 ± 0.7	5.8 ± 0.3		
TfO^-	10.2 ± 0.7	9.2 ± 0.4	11 ± 2 [b]	not detected [b]

[a] At 25 °C;[28] [b] at c = 0.1 M and 45 °C.[32]

remains constant (Fig. 5).

Solute Relaxation. The micelle-specific relaxations 1 & 2 were analyzed using Grosse's theory for charged colloids.[46] This model considers a dispersion of charged spherical particles of radius, R_G, and relative permittivity, ε_P, suspended in a medium of relative permittivity, ε_M, and dc conductivity, κ_M. An infinitely thin conducting layer with surface conductance λ_S, resulting from the lateral motion of condensed counterions, is assumed to be located at the surface of the charged particle. The latter is surrounded by a diffuse spherical cloud formed by the remaining dissociated (free) counterions and characterized by its Debye length, which in this model is approximated as

$$\chi^{-1} = \sqrt{\frac{\varepsilon_0 \varepsilon_M D}{\kappa_M}} \tag{10}$$

D is the diffusion coefficient of the free counterions.

Grosse showed that such a system exhibits two distinct dielectric relaxation processes and for small particle volume fractions, $\phi \ll 1$, assuming $R_G \gg \chi^{-1}$, he obtained analytical expressions for the amplitudes and relaxation times of both processes.[46] The lower-frequency mode, j = 1 of this study, arises from fluctuations of the diffuse ion cloud

with relaxation time

$$\tau_1 \approx \frac{R_G^2}{D} \tag{11}$$

and amplitude

$$S_1 = \frac{9\phi\varepsilon_M \left(\frac{2\chi\lambda_S}{\kappa_M}\right)^4}{16\left[\frac{2\chi\lambda_S}{\kappa_M}\left(\frac{2\lambda_S}{\kappa_M R_G}+1\right)+2\right]^2} \tag{12}$$

The higher-frequency mode, $j = 2$, is due to the tangential hopping motion, expressed as surface conductance, λ_S, of condensed counterions on the surface of the particle, located at R_G. Its relaxation time is given by

$$\tau_2 = \frac{\varepsilon_0\varepsilon_M\left(\frac{\varepsilon_P}{\varepsilon_M}+2\right)}{\kappa_M\left(\frac{2\lambda_S}{R_G\kappa_M}+2\right)} \tag{13}$$

and the corresponding amplitude is

$$S_2 = \frac{9\phi\varepsilon_M\left(\frac{2\lambda_S}{R_G\kappa_M}-\frac{\varepsilon_P}{\varepsilon_M}\right)^2}{\left(\frac{\varepsilon_P}{\varepsilon_M}+2\right)\left(\frac{2\lambda_S}{R_G\kappa_M}+2\right)^2} \tag{14}$$

The Grosse model assumes R_G as the effective radius of the micelle, *i.e.* also the layer occupied by the condensed counterions and the solvent therein is attributed to the micelle. Thus the corresponding volume fraction of micelles in the solution is given by

$$\phi = \frac{4}{3}\pi R_G^3 N_A \cdot \frac{c - cmc}{N} \tag{15}$$

with N as the aggregation number. This view is supported by a recently published combined DRS and SAXS study.[55] The surface conductance can be directly linked to a surface diffusion coefficient, D^S, of the bound counterions by

$$D^S = \frac{4\pi k_B T \lambda_S R_G^2}{\beta e_0^2 N} \tag{16}$$

where e_0 is the elementary chargeand β was taken from Table 1.[31]

Using the experimentally acquired relaxation parameters (τ_1, S_1, τ_2, S_2) as input data either all four equations of the Grosse model, eqs 11-14, or selections of them were simultaneously solved in a weighted fit (see Supporting Information for details) to yield the micelle-specific parameters Grosse radius, R_G, aggregation number, N, and surface conductance, λ_S. In this procedure the conductivity of the medium, κ_M, was set equal to the dc conductivity of the solution, *i.e.* $\kappa_M = \kappa(c)$. For the relative permittivity of the medium the value of pure water at 45 °C, $\varepsilon_M = 71.523$, was taken whereas $\varepsilon_P = 2$, typical for pure liquid hydrocarbons was assumed.[56] The diffusion coefficients of the free counterions, of charge number $z = -1$, at 45 °C were calculated according to

$$D = \frac{RT}{F^2} \cdot \frac{\lambda^\infty}{|z|} \tag{17}$$

from their ionic conductivities at infinite dilution, λ^∞, using published 25 °C values for the anions[56,57] scaled to 45 °C using Walden's rule.[58] In eq 17 F is the Faraday constant. Obtained values for D are (3.32, 3.26 & 1.89)$\times 10^{-9}$ m^{2}s^{-1} for Br^-, I^- & TfO^- respectively.

Table 4: Grosse radius, R_G, aggregation number, N, surface conductance, λ_S, surface diffusion coefficient, D^S, of the condensed counterions, and ratio D^S/D of the diffusion coefficients of condensed and free counterions for the investigated [C_{12}MIM]X micelles at 45 °C and for comparable [C_{12}TA]X micelles from the literature.

.

surfactant	$\frac{R_G}{10^{-9}\text{m}}$	N	$\frac{\lambda_S}{10^{-9}\Omega^{-1}}$	$\frac{D^S}{10^{-9}\text{m}^2\text{s}^{-1}}$	D^S/D
[C_{12}MIM]Br	1.83	29	3.59	1.40	0.42
[C_{12}MIM]I	2.32	72	3.64	0.76	0.23
[C_{12}MIM]TfO	2.88	180	2.05	0.26	0.14
[C_{12}TA]Br	2.17[a]	47[a]	2.43[a]	0.64[b]	0.32[b]
	2.26[c]	52[c]	3.00[c]	1.08[c]	0.37[c]
[C_{12}TA]TfO	2.21[c]	55[c,d]	2.12[c]	0.45[c]	0.27[c]

[a] Ref. 29 and [b] Ref. 31, both for 25 °C; [c] Ref. 32 (45 °C); [d] N fixed.

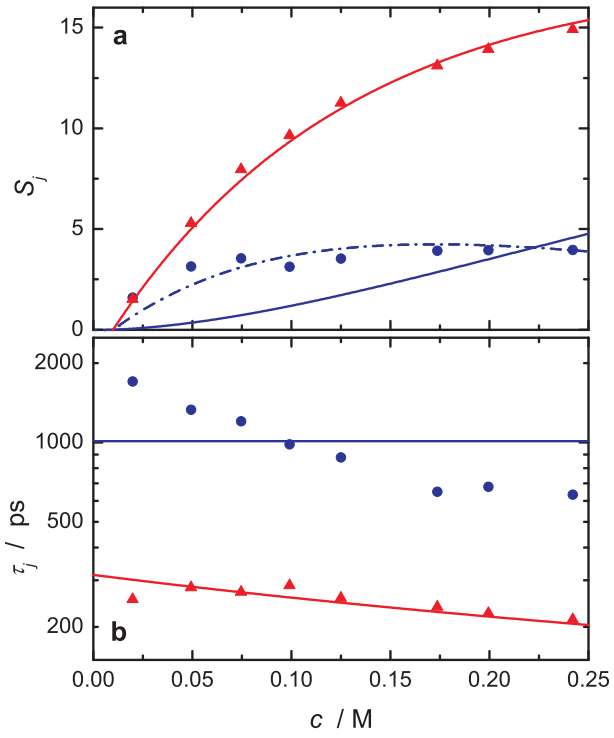

Figure 6: (a) Experimental amplitudes, S_j, and (b) relaxation times, τ_j, of the micellar relaxation processes $j = 1$ (●) and $j = 2$ (▲) of [C_{12}MIM]Br at 45 °C. The correspondingly colored lines represent the description with Grosse's model when S_1 is omitted in the fit. The dash-dotted line gives the fit of S_1 with adjusted Debye length, χ_{emp}^{-1}.

Figures 6, S12 & S13 show the outcome of these fits. For all three SAILs it turned out that, similar to sodium dodecylsulfate (SDS) solutions,[30] the Grosse model was not able to capture S_1 as the calculated amplitude had the wrong curvature. Additionally, τ_1 was largely overestimated when all four equations, eqs 11-14, were simultaneously solved, see Fig. S12. Significantly better descriptions of τ_1, τ_2 and S_2 were obtained when eq 12 was omitted. Since the Debye length only enters eq 12 and for SDS a good description of S_1 was obtained with an (albeit counter-intuitive) empirical modification[30] of χ^{-1} it is reasonable to assume that also for the present surfactants neither the conventional expression[58] for the Debye length nor Grosse's modification, eq 10, is valid. Accordingly, we focus the discussion on fits involving only eqs 11, 14 & 13, which yielded the Grosse radii, R_G, association numbers, N, and surface conductivities, λ_S, summarized in Table 4. However, note that with these R_G, N and λ_S values also a good description of the ion-cloud amplitude, S_1, can be achieved if for the effective Debye length a concentration dependence of the form

$$\chi_{emp}^{-1} = a_0 + a_1 \times c \tag{18}$$

is assumed (dash-dotted lines in Figs. 6, S12 & S13). The corresponding parameters, a_0 & a_1, are summarized in Table S13.

In the case of $[C_{12}MIM]Br$ the amplitude S_2 was well reproduced over the entire concentration region (Fig. 6). However, for the other two surfactants S_2 was systematically overestimated at $c \gtrsim 100$ mM (Figs. S12 & S13). Similar deviations were found for $[C_{12}TA]X$ solutions, albeit at significantly higher concentration.[29] The relaxation time of the surface-hopping mode, τ_2, was always well met but in particular for the bromide the experimental τ_1 values exhibit a marked decrease with c, whereas the Grosse model predicts a constant value.[59] This contrasts the behavior of $[C_{12}TA]X$ and SDS solutions where the experimental τ_1 does not vary much.[29,30,32]

Viscosity

Figure 7 reveals rather different rheological behavior of the three SAILs. The viscosity of [C_{12}MIM]Br solutions increases only weakly with concentration, whereas for [C_{12}MIM]I η considerably rises at c > 150 mM although the entire concentration range could still be fitted with an exponential function. In contrast to that, the viscosity of [C_{12}MIM]TfO solutions rapidly takes off at $c \approx 30$ mM, following a power law up to ~ 100 mM but then remains essentially constant. This suggest a gradual transition from spherical to rod-like micelles for the iodide, whereas for the triflate this transition is much sharper and apparently associated with a rapid growth of the average rod length.[60] According to Kern *et al.*[61] the subsequent plateau of η indicates that for triflate the maximum rod length is reached and orientational correlations among the micelles due to electrostatic interactions now dominate rheology.

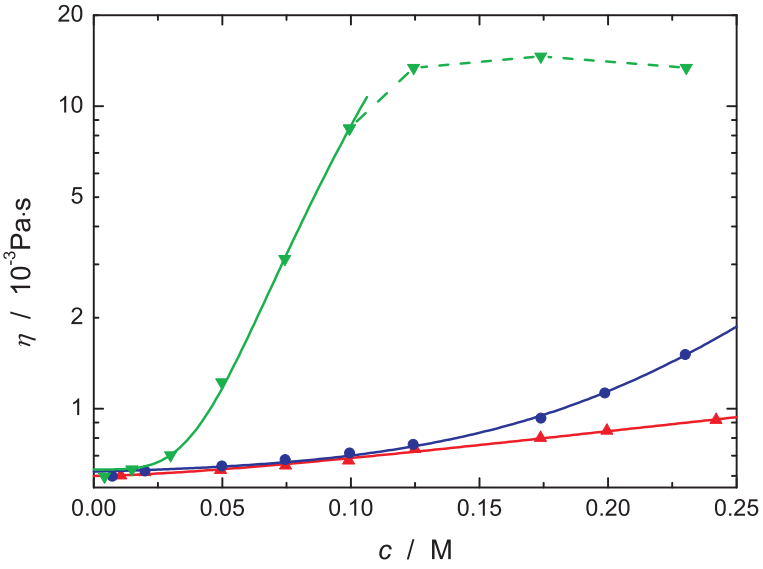

Figure 7: Viscosity, η, as function of solute concentration, c, of aqueous solutions of [C_{12}MIM]Br (▲), [C_{12}MIM]I (●) and [C_{12}MIM]TfO (▼) at 45 °C (lines as a guide to the eye, with solid lines representing fits with exponential functions).

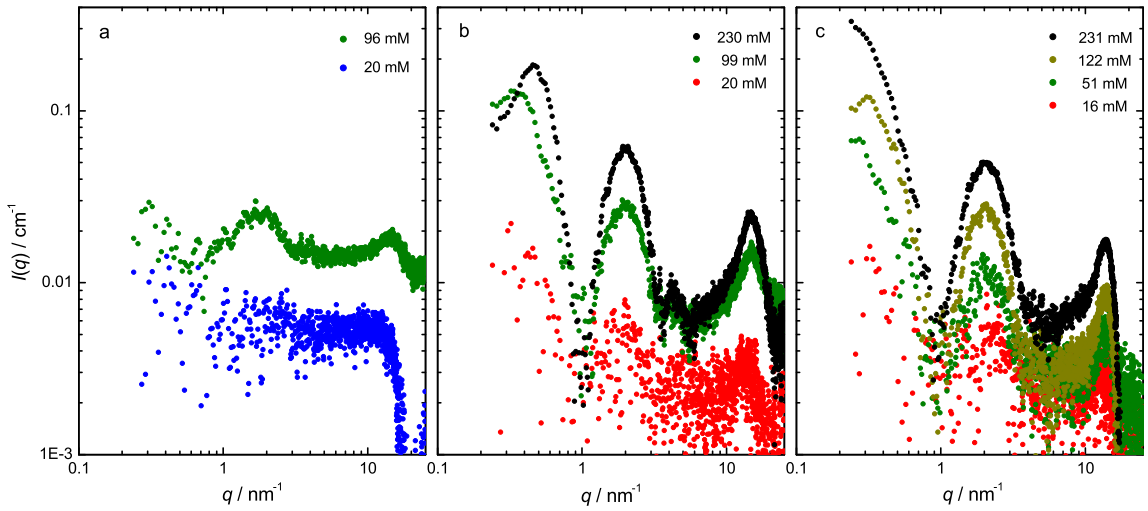

Figure 8: Small-and-wide angle X-ray scattering spectra of aqueous (a) $[C_{12}MIM]Br$, (b) $[C_{12}MIM]I$ and (c) $[C_{12}MIM]TfO$ solutions at room temperature. $I(q)$ is the absolute SWAXS intensity. The contribution of water to $I(q)$ was removed for clarity.

SWAXS

Figure 8 shows the obtained SWAXS spectra of aqueous $[C_{12}MIM]Br$ (panel a), $[C_{12}MIM]I$ (b) and $[C_{12}MIM]TfO$ (c) solutions, where the peak at 20 nm^{-1} associated with the O–O pair correlation of the solvent was subtracted for clarity. Due to the limited sensitivity of the instrument and the low scattering contrast of [C12MIM]Br micelles against H_2O, no change in the intensity compared to water was observed for $[C_{12}MIM]Br$ at the solute concentration of 20 mM but at 96 mM two weak oscillations at $q \approx 2\,nm^{-1}$ and (just detectable) ~4.2 nm^{-1} were found. Similar oscillations were also observed for iodide and triflate but much stronger and rapidly increasing with concentration. Such a scattering pattern is indicative for scatterers consisting of a core-shell system with excess electron density in the shell.[62–64] For the present $[C_{12}MIM]X$ micelles this observation reflects the high degree of counterion condensation, in particular for I^- and TfO^- (Table 1).

For $[C_{12}MIM]I$ and $[C_{12}MIM]TfO$ a strong rise of the scattering intensity was observed at $q < 1\,nm^{-1}$ when m exceeded 50 mM (Fig. 8b & c). This indicated formation of objects larger than ~ 5 to 10 nm. Their average radius clearly exceeded the radius of ~ 2.1 nm

expected for a spherical micelle of $[C_{12}MIM]^+$ ions from geometry.[65] Due to the limited q range of our instrument the region of constant $I(q)$ at $q \to 0$ was not reached and thus an unambiguous determination of the characteristic parameters of the scatterers impossible. Nevertheless, the obtained data support the inference from rheology of a transition from spherical to ellipsoidal or even rod-like micelles with increasing concentrations of $[C_{12}MIM]I$ and $[C_{12}MIM]TfO$.[62–64] For $[C_{12}MIM]Br$ solutions the very low scattering length density difference between micelles and solvent prevented detection of the characteristic low-q pattern by SWAXS but the small-angle neutron scattering study of Kusano *et al.*[66] provided clear evidence for the transition from spherical to ellipsoidal micelles also for this SAIL. However, with $R_{max}/R_{min} < 1.8$ the axis ratio remained small for $[C_{12}MIM]Br$ micelles. The latter finding probably explains the only moderate increase of the present viscosity data with c.

Discussion

Hydration. The results presented in Table 3 and Fig. 5 show that the total hydration numbers of all three SAILs are essentially the same and independent of concentration for $c \leq 250$ mM. By definition DRS hydration numbers, Z_i (i =t, s & ib), refer to one equivalent of solute and for salts are thus the sum of cation and anion contributions, Z_i^+ & Z_i^-. The present finding, $Z_t \approx 10 \ldots 12$, already suggests that the hydration of free anions might be negligible. Indeed, it is well known that the present anions are only weakly hydrated[50,52,53] Accordingly, previous DRS studies yielded $Z_t^- = 0$ for Br^- [26] and I^-.[67] To our knowledge no DRS data are available for TfO^- but $Z_t^- \approx 0$ can probably also be assumed for this ion.[32,53] The effective hydration numbers of Table 3 can thus be safely attributed to the micelles, more exactly: to the polar region formed by the cationic headgroups and condensed counterions. Interestingly, the present data significantly exceed the value of $Z_t^+ \approx 2$ found for the $[C_4MIM]^+$ cation, which does not form micelles.[68] This indicates a significant

degree of cooperativity in the hydration of $[C_{12}MIM]^+$ micelles. With regard to the total hydration number, Z_t, this cooperative effect does obviously not depend on the condensed anion. However, the amount of frozen water, expressed by Z_{ib}, varies markedly from nil for the TfO^- SAIL via increasingly relevant at $c > 125$ mM for Br^- to permanently present for I^-. This clearly indicates that at least for the two halide SAILs bound water molecules simultaneously interact with charged imidazolium headgroups of the micelle **and** condensed counterions and thus get trapped.

In that context, it is interesting to note that according to MD simulations even at a molar ratio of 1:200 of solute to solvent a significant fraction of the cations is still coordinated to anions in aqueous $[C_4MIM]Br$.[69] In these solutions, where no micelles are formed, H_2O molecules act as a bridge between anion and cation. Indications for such cooperative water binding by ion pairs also come from a Car-Parinello study[70] of aqueous $[C_2MIM]Cl$. Additionally, the formation of ib water for $[C_nTA]$-halide micelles was interpreted in that way.[28,32] Interestingly, however, the latter are much stronger hydrated than the present imidazolium micelles, with Z_t values of 20 to 27 and in particular $Z_{ib} \approx 10...14$, see Table 3. The large Z_t values for $[C_nTA]$ halide micelles indicated penetration of H_2O molecules beyond the rather flexible headgroup layer,[28,31] confirming thus information from other methods on these surfactants.[71–73] In contrast to that, Bhargava and Klein found no water molecules and counterions inside the quasi-spherical cation aggregates of $[C_nMIM]Br$ (n = 10, 12, 14, 16) forming spontaneously in their molecular dynamics simulations.[74] Apparently, the surface of $[C_{12}MIM]^+$ micelles is better "sealed" against water penetration (and as a consequence presumably more rigid). A possible reason might be $\pi - \pi$ interactions among the planar imidazolium rings which were found to be relevant for $[C_1MIM]Cl$ (albeit in the gas phase)[75] and for $[C_nMIM]Br$/*p*-xylene/water mixtures with n = 12, 14 & 16.[76] However, it must be noted that for binary aqueous $[C_nMIM]Br$ solutions such interactions were only identified for n = 16.[74]

Interestingly, the Z_t values of $[C_{12}MIM]TfO$ and $[C_{12}TA]TfO$ agree within error limits,

Table 3. Based on information from various techniques, Lima *et al.* suggested that in the case of $[C_{12}TA]TfO$ the slightly amphiphilic triflate anions insert into the headgroup layer, leading to large disc-shaped micelles with a rather "sealed" surface in contact with the solvent.[32,33,77] Hydration is thus reduced here mainly for steric reasons. A similar situation may apply also for $[C_{12}MIM]TfO$ although the observed rheology (Fig. 7) suggests rod-like micelles for this surfactant. Obviously, DRS cannot directly monitor whether triflate anions insert into the imidazolium layer but it is interesting to note that in contrast to the other SAILs no ib water was found. Instead, the retardation factor, $r = \tau_3/\tau_4 \approx 18$, for the hydrating slow H_2O molecules is rather large and independent of T and c. Their activation enthalpy, $\Delta H^{\neq}(\tau_3)$, of this mode is similar to bulk water, thus the binding strength to the micelle surface is similar to H_2O-H_2O interactions. On the other hand, the activation entropy is definitely smaller than the bulk value, if not even negative (Table 2). This suggests that —in contrast to the halide SAILs— for $[C_{12}MIM]TfO$ the large r value arises from a shielding of the hydrating H_2O against approaching new H-bond partners by the micelles. Accordingly, τ_3 is here dominated by the volume excluded to the rotation of these water molecules.[50]

For the halide SAILs $\Delta H^{\neq}(\tau_3) > \Delta H^{\neq}(\tau_4)$ (Table 2). Whilst for the iodide the activation enthalpy of the slow-water relaxation exceeds the bulk-water value only by ~40 % with a moderate and roughly constant retardation factor of $r \approx 6$, $\Delta H^{\neq}(\tau_3)$ is five times larger for the bromide with a strongly T-dependent retardation factor, dropping from $r \approx 39$ at 25 °C to ~3.3 at 65 °C. For both SAILs the activation entropy of τ_3 is clearly positive, suggesting that the transition state for the rotation of these hydrating H_2O molecules is less "ordered". Thus, hydrogen-bond breaking is probably involved in the rate-determining step. Keeping in mind that, similar to aqueous $[C_4MIM]Br$[69] and $[C_2MIM]Cl$,[70] the involved H_2O molecules probably bind simultaneously to a cation in the headgroup layer and a condensed anion sitting on top of that, this would also explain the high $\Delta H^{\neq}(\tau_3)$ values. However, without detailed molecular-level information, *e.g.* from MD simulations

or time-resolved vibrational spectroscopy, this remains speculation as does an answer to the question why for I^- ib water is observed over the entire concentration range whereas for Br^- this becomes detectably only for $c > 125$ mM. In any case, hydration seems to be a "local" property of the micelle surface which does not reflect the apparently large variation of micelle shape with c for $[C_{12}MIM]I$ and in particular for $[C_{12}MIM]TfO$ that is suggested by the rheological behavior of these SAILs (Fig. 7).

Micelle Properties. The estimated Grosse radii, R_G, and aggregation numbers, N, rise in the order of $[C_{12}MIM]Br < [C_{12}MIM]I < [C_{12}MIM]TfO$ (Table 4). The surface conductivities, λ_S, of the bromide and iodide SAILs are practically the same but that of the triflate is significantly reduced. This is compatible with the assumption that, similar to $[C_{12}TA]TfO$,[32,33,77] also for $[C_{12}MIM]TfO$ micelles the condensed anions are inserted in the headgroup layer. Compared to their bulk values the diffusion coefficients of the anions on the micelle surface are always considerably reduced, with D^S/D decreasing in the order $Br^- > I^- > TfO^-$.

Grosse theory[46] assumes micelles to be spherical, with R_G giving the location of the center of the condensed counterions relative to the center of the micelles. The Debye length should be negligible compared to R_G and micelle-micelle interactions absent. Clearly, these conditions are not really met by the present SAIL solutions. The observed rheology (Fig. 7) and the SWAXS data (Fig. 8) suggest non-spherical micelles for the iodide and, in particular, for the triflate. Additionally, in the covered concentration range $R_G < \chi^{-1}$ in all cases. Even more, almost from the *cmc* the average center-to-center distance, d, of (assumed spherical) micelles with aggregation number N (Table 4) is smaller than $2(R_G + \chi^{-1})$ (Fig. 9). Thus, ion clouds overlap and therefore micelle-micelle interactions are present. This probably explains why the ion-cloud amplitude, S_1, cannot be reproduced with eq 10 or the conventional expression[58] for χ^{-1} but also raises the question how relevant the present Grosse parameters, Table 4, are. As discussed below, it turns out that indeed useful information can be extracted from the analysis of the two micelle-specific modes.

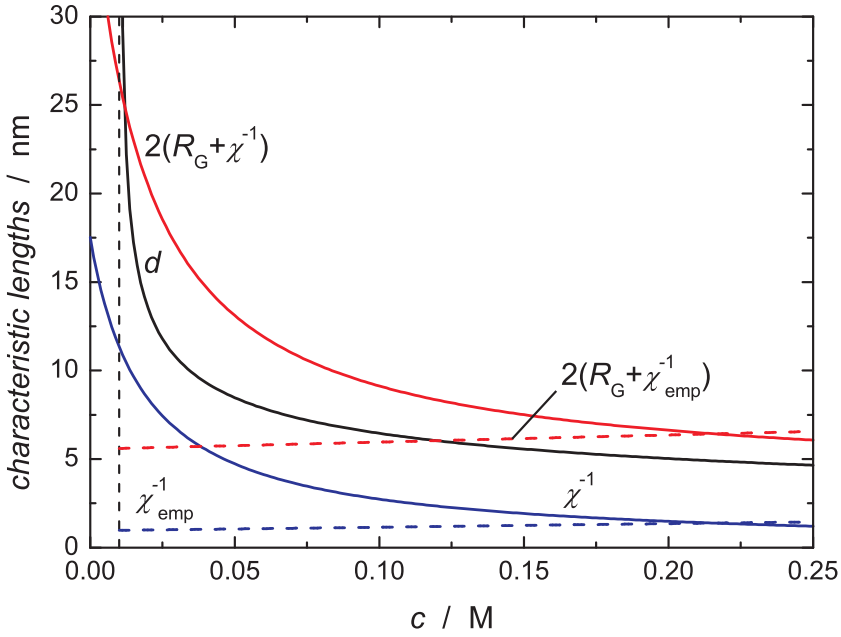

Figure 9: Characteristic lengths in aqueous [C_{12}MIM]Br solutions assuming spherical micelles of aggregation number N = 29: micelle center-to-center distance, d; Debye length according to eq 10, χ^{-1}, and empirical value derived from S_1 with eq 12, χ_{emp}^{-1}; effective micelle diameters, $2(R_G + \chi^{-1})$ and $2(R_G + \chi_{emp}^{-1})$.

For [C_{12}MIM]Br a number of literature data on micelle size and shape are available. Using luminescence quenching Vanyur *et al.*[78] and Wang et al.[79] reported N = 44, whereas Šarac *et al.*[16] determined a value of 16.82 with conductivity measurements. According to the MD simulations of Bhargava *et al.*[74] [C_{12}MIM]Br forms quasi-spherical but rather open aggregates with a most probable aggregation number of N = 22 at c = 716 mM. This contrasts the small-angle neutron scattering (SANS) results of Kusano *et al.*,[66] where micelles change from spherical (N = 85.96) at 42.5 mM to ellipsoidal at $c \geq$ 91.6 mM, reaching an axis ratio of 1.74 and an aggregation number of 154.3 at 1040 mM. With ~2.0 nm the minor radius of the ellipsoid found in that study remains practically constant and is somewhat shorter than the length of a stretched cation, 2.10 nm,[80] but significantly larger than the present R_G value of 1.83 nm. Cognigni *et al.* did not report aggregation numbers but deduced an effective radius increasing from 2.24 nm at 25 mM to 2.57 nm at 100 mM with constant core radius, ~0.97 nm, for the spherical core-shell model fitted to

their SAXS data.[2]

Obviously, the aggregation number of [C_{12}MIM]Br micelles is not well known. In part, this certainly reflects that reported values were determined at different concentrations but certainly more relevant is the applied method. On the other hand, there seems to be consensus on the spherical shape of [C_{12}MIM]Br micelles close to *cmc*. According to Kusano *et al.*[66] the aggregates get more and more ellipsoidal with rising surfactant concentration but even at 1040 M the micelles are far from cylindrical shape. This explains why viscosity rises only weakly with c for this compound (Fig. 7) despite expected micelle-micelle interactions (Fig. 9). In the concentration range covered by the present investigation, $c < 250$ mM, the axis ratio of the ellipsoidal micelles reaches ~1.6 at maximum.[66] Apparently, this is close enough to spherical for the assumptions of Grosse's theory[46] as amplitude, S_2, and relaxation time, τ_2, of the mode solely governed by micelle-specific parameters (N = 29, R_G = 1.83 nm, $\lambda_S = 3.59 \times 10^{-9}\,\Omega^{-1}$) are well described by eqs 14 & 13 at all c (Fig. 6).

Compared to the data for [C_{12}TA]Br (Table 4) the present values for N and R_G of [C_{12}MIM]Br are rather low. In Fig. 10 the corresponding effective volume fraction of micelles, calculated with eq 15 is compared with the result

$$\phi(c) = \frac{c_b(cmc) - c_b(c)}{c_w(0)} \tag{19}$$

obtained from the DRS-detected concentration of bulk-like water, c_b.[28] Except for the highest concentration the two independent approaches yield the same ϕ values for [C_{12}MIM]Br micelles. A similar agreement was previously obtained for the much better characterized [C_{12}TA]Br micelles,[31] lending thus credit to the Grosse parameters of Table 4 and the assumption of essentially spherical aggregates up to 250 mM for this imidazolium SAIL.

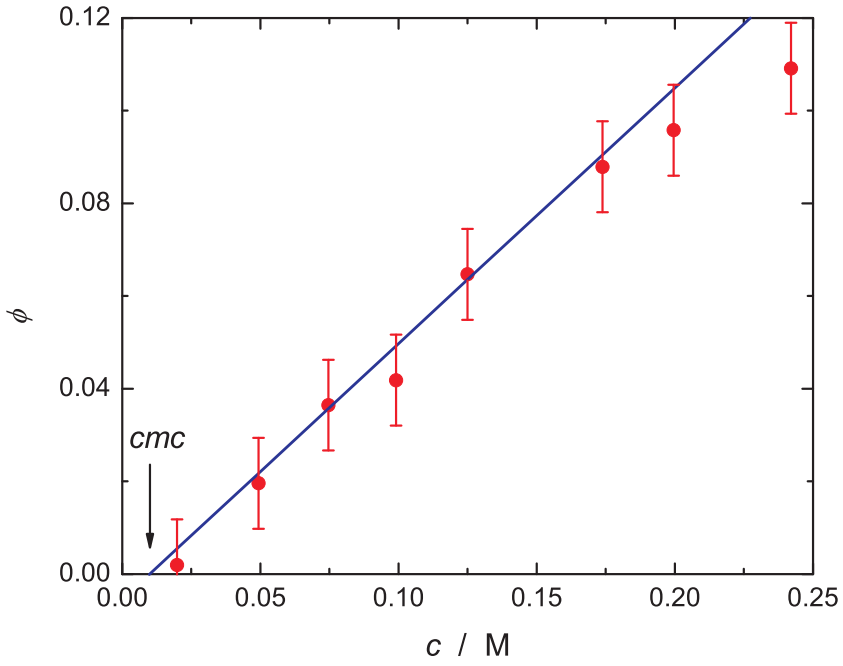

Figure 10: Effective volume fraction, ϕ, of [C_{12}MIM]Br micelles in aqueous solution calculated from Grosse radius, R_G, and aggregation number, N, with eq 15 (solid line), and independently from the bulk water amplitude, S_b, via eq 19 (●).

Further support for the present R_G and N values of [C_{12}MIM]Br comes from the favorable comparison of the associated effective monomer volume, $V_G^m = (4\pi R_G^3)/(3N) = 0.855\,nm^3$ (Table 5) with the volume of the bare, $V_\phi^m = V_\phi^{mic}/N_A$, and the hydrated monomer

$$V_{\phi,hyd}^m = \left[V_\phi^{mic} + Z_t \times V^\circ(H_2O)\right]/N_A \qquad (20)$$

calculated from the apparent molar volume of the surfactant in the micelle, V_ϕ^{mic}, and the molar volume of water at 45 °C, $V^\circ(H_2O) = 18.193\,cm^3mol^{-1}$ (Table 5).[81] Note that for [C_{12}MIM]Br the difference between V_G^m and $V_{\phi,hyd}^m$ corresponds to a single additional hydrating H_2O molecule, which is within the uncertainty of Z_t for this surfactant.

To the best of our knowledge no numerical information on the size and shape of [C_{12}MIM]I and [C_{12}MIM]TfO micelles is available in the literature. Also the present SWAXS data (Fig. 8) did not allow reliable extraction of this information. Using isothermal titration calorimetry, Šarac *et al.*[16] obtained aggregation numbers of 17.6 for the first and of

Table 5: Effective monomer volume in the micelle from Grosse's model, V_G^m, and molecular volumes V_ϕ^m and $V_{\phi,hyd}^m$ calculated from the apparent molar volume of the micelle without and with taking micelle hydration into account, see text.

.

surfactant	$\frac{V_G^m}{nm^3}$	$\frac{V_\phi^m}{nm^3}$	$\frac{V_{\phi,hyd}^m}{nm^3}$
$[C_{12}MIM]Br$	0.855	0.511	0.825
$[C_{12}MIM]I$	0.726	0.532	0.889
$[C_{12}MIM]TfO$	0.556	0.598	0.907

16.9 for the second SAIL but judging from the available data for the bromide surfactant, see above, these numbers appear to be rather small. On the other hand, also the present N and R_G values (Table 4) for $[C_{12}MIM]I$ and in particular for $[C_{12}MIM]TfO$ are unrealistic because only at low c the effective volume fraction of micelles, ϕ, derived from the bulk-water amplitude, eq 19, agrees with that derived from the Grosse radius, eq 15. With increasing concentration the values obtained from S_b grow considerably faster than those calculated from the micelle relaxation (Figs. S14 & S15). By the same token, the effective monomer volumes, V_G^m, calculated from R_G and N are significantly smaller than the $V_{\phi,hyd}^m$ values obtained from apparent molar volumes (Table 5). Since the Grosse model also failed reproducing S_2 at $c > 75$ mM for $[C_{12}MIM]I$ (Fig. S12) and $c > 125$ mM for $[C_{12}MIM]TfO$ (Fig. S13), these observations are probably a consequence of the tendency of these surfactants to form rod-like micelles, as suggested by their rheology (Fig. 7) and SWAXS data (Fig. 8). Due to the limited data base no systematic study of the impact of micelle shape on surface conductance, λ_S, and diffusion coefficient, D^S, is possible yet but almost certainly the values (Table 4) for $[C_{12}MIM]I$ and $[C_{12}MIM]TfO$ are unreliable at $c > 75$ mM respectively 125 mM.

At 25 °C a linear correlation between the relative surface diffusion coefficient, D^S/D, and the degree of counterion dissociation, $1 - \beta$, was observed for $[C_nTA]X$ surfactants with halide anions.[31] Interestingly, the present data for $[C_{12}MIM]Br$ and $[C_{12}MIM]I$ together

with those for [C_{12}TA]Cl and [C_{12}TA]Br at 45 °C[32] form a straight line shifted parallel to the room-temperature data (Fig. S16), whereas those for [C_{12}MIM]TfO, [C_{12}TA]TfO and [C_{12}TA]MS (MS: methylsulfate) are off, with both triflates in opposite directions. The increase of D^S/D with $(1-\beta)$ appears reasonable as reduced counterion condensation means more unoccupied and thus accessible binding sites for the hopping anions. [C_{12}TA]TfO micelles are disk-shaped with the triflate counterions inserted in the headgroup layer,[73,77] whereas the present rheological data (Fig. 7) suggest rods for [C_{12}MIM]TfO.[60,61] This may explain their opposing deviations in Fig. S16. In any case, for [C_{12}MIM]TfO the surface diffusion coefficient of the anion is significantly smaller than that of the two studied halides, suggesting insertion of TfO^- anions into the headgroup layer.

As already indicated, the ion-cloud amplitude, S_1, cannot be reproduced with eq 10 or the conventional expression[58] for χ^{-1} (Figs. 6, S12 & S13). For micellar solutions of SDS it was found that the assumption of a linearly increasing Debye length, eq 18, provided an excellent description of S_1 over the entire concentration range studied.[30] This was also the case for [C_{12}MIM]Br, Fig. 6. For the two other SAILs the fit was excellent for $c < 150$ mM but then the experimental S_1 deviated from the prediction, Figs. S12 & S13. However, in all three cases eq 18 predicts the correct concave curvature of the experimental data. The intercepts, a_0, and slopes, a_1, obtained by fitting S_1 with eq 12, using the R_G and N values of Table 4 as fixed input, are summarized in Table S13. Most noteworthy, this empirical expression for χ^{-1} does not show the marked decrease with rising c expected from Debye theory but a weak increase, reaching the values given by eq 10 only at $c \approx 200$ mM (Fig. 9). As a consequence, the average separation, d, of the micelles exceeds the effective micelle diameter, $2(R_G + \chi^{-1}_{emp})$, at $c \lesssim 100$ mM for all three SAILs. At present, it cannot be decided whether the need for eq 18 to describe S_1 indicates a general failure of the Grosse model or if at low c Coulomb screening is indeed much weaker for these micelles than conventionally predicted. However, it should be noted that, based on surface-force measurements between charged plates, a recent scaling analysis suggested that also for

concentrated electrolyte solutions the characteristic length of charge screening, *i.e.* the effective Debye length, increases linearly with concentration.[82]

Concluding Remarks

For the investigated $[C_{12}MIM]X$ SAILs the effective total hydration numbers, Z_t^0 (Table 3, Fig. 5), determined from the bulk-water amplitude can be safely assigned to the micelles as the free anions are only weakly hydrated and contributions of the free cations are negligible because of the small *cmc*. All three surfactants bind approximately 10-11 H_2O molecules per imidazolium headgroup. However, there are differences in binding quality. Whilst for the triflate SAIL all bound water is only retarded by a factor of $r \approx 18$, approximately half of the hydrating H_2O is completely frozen (ib) for $[C_{12}MIM]I$. The bromide SAIL is intermediate as here ib water was detected only for $c > 150$ mM but for lower c solvent retardation is very large ($r \approx 39$) at room temperature. Counterion condensation is much stronger for TfO^- compared to Br^- and I^- (Table 1). At the same time, the surface diffusion coefficient of triflate is much smaller (Table 4). Possibly, this suggests that, similar to $[C_{12}TA]TfO$,[73,77] also for $[C_{12}MIM]TfO$ the condensed counterions are inserted into the headgroup layer. Halide ions apparently sit on top of the micelles with ib water molecules simultaneously binding to them and the imidazolium cations, comparable to the situation for aqueous $[C_2MIM]Cl$[70] and $[C_4MIM]Br$.[69]

Analysis of the two micelle-specific relaxations suggests that —within the sensitivity of Grosse's model— $[C_{12}MIM]Br$ micelles remain essentially spherical in the investigated concentration range. Viscosity data (Fig. 7) but also Grosse radii and aggregation numbers (Table 4), as well as volumetric data (Table 5) indicate that this is not the case for the other two SAILs. In particular $[C_{12}MIM]TfO$ almost certainly forms rod-like micelles (Fig. 8). Apparently for all three surfactants micelle-micelle distances are so small that Grosse's (but also the conventional) expression, eq 10, for the Debye screening length breaks down.

Recently, some of us observed that micelles of $[C_{12}MIM]X$ SAILs were promising catalysts for nucleophilic substitution reactions.[2] However, at least for the chosen model reaction of nitrophenyl diphenyl phosphate (PNPDPP, assumed to be solubilized in the micelle) with acetaldoxime, the catalytic activity strongly depended on the counterion, dropping from a 34-fold rate enhancement for Cl^-, compared to the non-catalyzed reaction, to only 2.3-fold for TfO^-. At least for the halides it appears that the superior performance of $[C_{12}MIM]X$ micelles is due to their weaker hydration compared to $[C_{12}TA]X$ (Table 3), permitting thus easier access of the acetaldoxime anions dissolved in the aqueous phase to the PNPDPP molecules sitting in the micelle. By the same token, due to the increasing condensation of counterions and their simultaneously decreasing mobility (Tables 1 & 4) the surface-charge density of the cationic $[C_{12}MIM]$ micelle becomes less positive and thus less attractive for the aldoxime anion when going from Br^- via I^- to TfO^- as the surfactant counterion in the $[C_{12}MIM]X$ series.

Acknowledgement

The authors thank Pierre Bauduin, Olivier Diat and Bruno Corso for their help with SWAXS measurements. Financial support from the COST action no. CM1206, *Exchange on Ionic Liquids*, is gratefully acknowledged. KB also acknowledges financial support by the Austrian Science Fund (FWF) with grant no. P25504-N28 and TB thanks the BFHZ (Bayerisch-französisches Hochschulzentrum) for grant FK41_15, covering travel expenses, and the DFG Graduate School GRK1626, Chemical Photocatalysis, for financial support.

Supporting Information Available

Tables with data for density, viscosity and conductivity of the investigated solutions. Tables with parameters of the D+D+D+D model fitted to the dielectric spectra and additional Figures illustrating data analysis. This material is available free of charge via the Internet

at http://pubs.acs.org/.

Notes and References

(1) Bica, K.; Gärtner, P.; Gritsch, P. J.; Ressmann, A. K.; Schröder, C.; Zirbs, R. Micellar Catalysis in Aqueous-Ionic Liquid Systems. *Chem. Commun.* **2012**, *48*, 5013–5015.

(2) Cognigni, A.; Gärtner, P.; Zirbs, R.; Peterlik, H.; Prochazka, K.; Schröder, C.; Bica, K. Surface-active Ionic Liquids in Micellar Catalysis: Impact of Anion Selection on Reaction Rates in Nucleophilic Substitutions. *Phys. Chem. Chem. Phys.* **2016**, *18*, 13375–13384.

(3) Walden, P. Molecular Weights and Electrical Conductivity of Several Fused Salts. *Bulletin of the Russian Academy of Sciences: Physics* **1914**, 405–422.

(4) Seddon, K. R.; Stark, A.; Torres, M.-J. Influence of Chloride, Water, and Organic Solvents on the Physical Properties of Ionic Liquids. *Pure Appl. Chem.* **2000**, *72*, 2275–2287.

(5) Welton, T. Room-Temperature Ionic Liquids. Solvents for Synthesis and Catalysis. *Chem. Rev.* **1999**, *99*, 2071–2084.

(6) Wasserscheid, P.; Welton, T. *Ionic Liquids in Synthesis*; Wiley-VCH, 2007.

(7) Plechkova, N. V.; Seddon, K. R. Applications of Ionic Liquids in the Chemical Industry. *Chem. Soc. Rev.* **2007**, *37*, 123–150.

(8) Kohno, Y.; Ohno, H. Ionic Liquid/Water Mixtures: From Hostility to Conciliation. *Chem. Commun.* **2012**, *48*, 7119–7130.

(9) Chaban, V. V.; Prezhdo, O. V. Ionic and Molecular Liquids: Working Together for Robust Engineering. *J. Phys. Chem. Lett.* **2013**, *4*, 1423–1431.

(10) Hayes, R.; Warr, G. G.; Atkin, R. Structure and Nanostructure in Ionic Liquids. *Chem. Rev.* **2015**, *115*, 6357–6426.

(11) Bruce, D. W.; Cabry, C. P.; Canongia Lopes, J. N.; Costen, M. L.; D'Andrea, L.; Grillo, I.; Marshall, P. C.; McKendrick, K. G.; Minton, T. K.; Purcell, S. M.; Rogers, S.; Slattery, J. M.; Shimizu, K.; Smoll, E.; Tesa-Serrate, M. A. Nanosegregation and Structuring in the Bulk and at the Surface of Ionic-Liquid Mixtures. *J. Phys. Chem. B* **2017**, *121*, 6002–6020.

(12) Greaves, T. L.; Drummond, C. J. Solvent Nanostructure, the Solvophobic Effect and Amphiphile Self-assembly in Ionic Liquids. *Chem. Soc. Rev.* **2013**, *42*, 1096–1120.

(13) Blesic, M.; Marques, M. H.; Plechkova, N. V.; Seddon, K. R.; Rebelo, L. P. N.; Lopes, A. Self-aggregation of Ionic Liquids: Micelle Formation in Aqueous Solution. *Green Chem.* **2007**, *9*, 481–490.

(14) Łuczak, J.; Hupka, J.; Thöming, J.; Jungnickel, C. Self-organization of Imidazolium Ionic Liquids in Aqueous Solution. *Colloids Surf., A* **2008**, *329*, 125–133.

(15) Tariq, M.; Freire, M. G.; Saramago, B.; Coutinho, J. A. P.; Canongia Lopes, J. N.; Rebelo, L. P. N. Surface Tension of Ionic Liquids and Ionic Liquid Solutions. *Chem. Soc. Rev. 41*, 829–868.

(16) Šarac, B.; Medoš, Ž.; Cognigni, A.; Bica, K.; Chen, L.-J.; Bešter-Rogač, M. Thermodynamic Study for Micellization of Imidazolium Based Surfaceactive Ionic Liquids in Water: Effect of Alkyl Chain Length and Anions. *Colloids Surf. A: Physicochem. Eng. Aspects* **2017**, *http://dx.doi.org/10.1016/j.colsurfa.2017.01.062*.

(17) Tanford, C. *The Hydrophobic Effect: Formation of Micelles and Biological Membranes*; Wiley: New York, 1980.

(18) Łuczak, J.; Jungnickel, C.; Markiewicz, M.; Hupka, J. Solubilization of benzene, toluene, and xylene (BTX) in aqueous micellar solutions of amphiphilic imidazolium ionic liquids. *J. Phys. Chem. B* **2013**, *117*, 5653–5658.

(19) Svinyarov, I.; Bogdanov, M. G. Ionic Liquid-assisted Micellar Extraction for the Quantitative Determination of Sesquiterpenic Acids in *Valeriana officinalis* L. (Caprifoliaceae). *Sep. Sci. Technol.* **2017**, *http://dx.doi.org/10.1080/01496395.2017.1295995*.

(20) Nowicki, J.; Łuczak, J.; Stańczyk, D. Dual functionality of amphiphilic 1-alkyl-3-methylimidazolium hydrogen sulfate ionic liquids: surfactants with catalytic function. *RSC Adv.* **2016**, *6*, 11591–11601.

(21) Cokoja, M.; Reich, R. M.; Wilhelm, M. E.; Kaposi, M.; Schäffer, J.; Morris, D. S.; Münchmeyer, C. J.; Anthofer, M. H.; Markovits, I. I. E.; Kühn, F. E.; Herrmann, W. A.; Jess, A.; Love, J. B. Olefin epoxidation in aqueous phase using ionic-liquid catalysts. *ChemSusChem* **2016**, *9*, 1773–1776.

(22) Cognigni, A.; Kampichler, S.; Bica, K. Surface-active ionic liquids in catalysis: Impact of structure and concentration on the aerobic oxidation of octanol in water. *J. Coll. Interface. Sci.* **2017**, *492*, 136–145.

(23) Evans, D. F.; Wennerström, H. *The Colloidal Domain*, 2nd ed.; Wiley-VCH: New York, 1999.

(24) Kremer, F.; Schönhals, A. *Broadband Dielectric Spectroscopy*; Springer: Berlin, 2002.

(25) Stoppa, A.; Nazet, A.; Buchner, R.; Thoman, A.; Walther, M. Dielectric Response and Collective Dynamics of Acetonitrile. *J. Mol. Liq.* **2015**, *212*, 963–968.

(26) Buchner, R.; Hefter, G. Interactions and Dynamics in Electrolyte Solutions by Dielectric Spectroscopy. *Phys. Chem. Chem. Phys.* **2009**, *11*, 8984–8999.

(27) Eiberweiser, A.; Nazet, A.; Hefter, G.; Buchner, R. Ion Hydration and Association in Aqueous Potassium Phosphate Solutions. *J. Phys. Chem. B* **2015**, *119*, 5270–5281.

(28) Baar, C.; Buchner, R.; Kunz, W. Dielectric Relaxation of Cationic Surfactants in Aqueous Solution. 1. Solvent Relaxation. *J. Phys. Chem. B* **2001**, *105*, 2906–2913.

(29) Baar, C.; Buchner, R.; Kunz, W. Dielectric Relaxation of Cationic Surfactants in Aqueous Solution. 2. Solute Relaxation. *J. Phys. Chem. B* **2001**, *105*, 2914–2922.

(30) Fernandez, P.; Schrödle, S.; Buchner, R.; Kunz, W. Micelle and Solvent Relaxation in Aqueous Sodium Dodecylsulfate Solutions. *ChemPhysChem* **2003**, *4*, 1065–1072.

(31) Buchner, R.; Baar, C.; Fernandez, P.; Schrödle, S.; Kunz, W. Dielectric Spectroscopy of Micelle Hydration and Dynamics in Aqueous Ionic Surfactant Solutions. *J. Mol. Liq.* **2005**, *118*, 179–187.

(32) Lima, F. S.; Chaimovich, H.; Cuccovia, I. M.; Buchner, R. Dielectric Relaxation Spectroscopy Shows a Sparingly Hydrated Interface and Low Counterion Mobility in Triflate Micelles. *Langmuir* **2013**, *29*, 10037–10046.

(33) Lima, F. S.; Cuccovia, I. M.; Buchner, R.; Antunes, F. E.; Lindman, B.; Miguel, M. G.; Horinek, D.; Chaimovich, H. Sodium Triflate Decreases Interaggregate Repulsion and Induces Phase Separation in Cationic Micelles. *Langmuir* **2015**, *31*, 2609–2614.

(34) Glasstone, S.; Laidler, K. J.; Eyring, H. *The theory of rate processes*; McGraw Hill: New York, 1941.

(35) Huddleston, J. G.; Willauer, H. D.; Swatloski, R. P.; Visser, A. E.; Rogers, R. D. Room Temperature Ionic Liquids as Novel Media for 'Clean' Liquid-liquid Extraction. *Chem. Commun.* **1998**, *16*, 1765–1766.

(36) Souza, B. S.; Leopoldino, E. C.; Tondo, D. W.; Dupont, J.; Nome, F. Imidazolium-Based

Zwitterionic Surfactant: A New Amphiphilic Pd Nanoparticle Stabilizing Agent. *Langmuir* **2012**, *28*, 833–840.

(37) Nazet, A.; Sokolov, S.; Sonnleitner, T.; Makino, T.; Kanakubo, M.; Buchner, R. Densities, Viscosities, and Conductivities of the Imidazolium Ionic Liquids [Emim][Ac], [Emim][FAP], [Bmim][BETI], [Bmim][FSI], [Hmim][TFSI], and [Omim][TFSI]. *J. Chem. Eng. Data* **2015**, *60*, 2400–2411.

(38) Zana, R. Ionization of Cationic Micelles: Effect of the Detergent Structure. *J. Colloid Interface Sci.* **1980**, *78*, 330–337.

(39) Buchecker, T.; Krickl, S.; Winkler, R.; Grillo, I.; Bauduin, P.; Touraud, D.; Pfitzner, A.; Kunz, W. The Impact of the Structuring of Hydrotropes in Water on the Mesoscale Solubilisation of a Third Hydrophobic Component. *Phys. Chem. Chem. Phys.* **2017**, *19*, 1806–1816.

(40) Hammersley, A. P. FIT2D: an introduction and overview. *European Synchrotron Radiation Facility Internal Report ESRF97HA02T* **1997**, *68*.

(41) Ao, M.; Kim, D. Aggregation Behavior of Aqueous Solutions of 1-Dodecyl-3-methylimidazolium Salts with Different Halide Anions. *J. Chem. Eng. Data* **2013**, *58*, 1529–1534.

(42) Böttcher, C. F. J.; Bordewijk, P. *Theory of Electric Polarization, Vol. 2*; Elsevier: Amsterdam, 1978.

(43) Sonnleitner, T.; Turton, D. A.; Waselikowski, S.; Hunger, J.; Stoppa, A.; Walther, M.; Wynne, K.; Buchner, R. Dynamics of RTILs: A Comparative Dielectric and OKE Study. *J. Mol. Liq.* **2014**, *192*, 19–25.

(44) Zasetsky, A. Y.; Buchner, R. Quasi-linear Least Squares and Computer Code for

Numerical Evaluation of Relaxation Time Distribution from Broadband Dielectric Spectra. *J. Phys.: Condens. Matter* **2011**, *23*, 025903.

(45) Data for $0.1 \leq \nu/\mathrm{GHz} \leq 89$ from this laboratory[83,84] were extended to 2 THz by interpolated data of Rønne *et al.*[85] The thus obtained spectrum was fitted to a D+D model, keeping the static permittivity fixed to $\varepsilon_s(0) = 71.523$.[86] Obtained parameters for 45 °C are $S_1 = S_c = 66.113$, $\tau_1 = \tau_c = 5.33$ ps, $S_2 = S_f = 2.63$, $\tau_2 = \tau_f = 0.165$ ps and $\varepsilon_\infty = 2.78$.

(46) Grosse, C. Permittivity of a Suspension of Charged Spherical Particles in Electrolyte Solution. 2. Influence of the Surface Conductivity and Asymmetry of the Electrolyte on the Low- and High-frequency Relaxations. *J. Phys. Chem.* **1988**, *92*, 3905–3910.

(47) Zana, R. Critical Micellization Concentration of Surfactants in Aqueous Solution and Free Energy of Micellization. *Langmuir* **1996**, *12*, 1208–1211.

(48) Assuming an effective dipole moment of 5.05 D (MOPAC, COSMO-PM6 functional) for TfO^- the relaxation amplitude at the highest concentration, $c = 250$ mM, is ~0.14 and thus negligible within experimental uncertainty.

(49) Buchner, R.; Barthel, J.; Stauber, J. The Dielectric Relaxation of Water between 0 °C and 35 °C. *Chem. Phys. Lett.* **1999**, *306*, 57–63.

(50) Laage, D.; Stirnemann, G.; Sterpone, F.; Rey, R.; Hynes, J. T. Reorientation and Allied Dynamics in Water and Aqueous Solutions. *Annu. Rev. Phys. Chem.* **2011**, *62*, 395–416.

(51) For pure water, where very precise data are available, plots of τ_s and η *vs.* T^{-1} are notably curved, suggesting a temperature dependence of $\Delta H^{\neq}$ and $\Delta S^{\neq}$ as discussed in Ref. 49.

(52) Migliorati, V.; Sessa, F.; Aquilanti, G.; D'Angelo, P. Unraveling Halide Hydration: A High Dilution Approach. *J. Chem. Phys.* **2014**, *141*, 044509.

(53) Bergström, P.-Å.; Lindgren, J. An Infrared Spectroscopic Study of the Hydration of the Triflate Ion ($CF_3SO_3^-$) in Aqueous Solution. *J. Mol. Struct.* **1990**, *239*, 103–111.

(54) Hubbard, J. B.; Colonomos, P.; Wolynes, P. G. Molecular theory of solvated ion dynamics. III. The kinetic dielectric decrement. *J. Chem. Phys.* **1979**, *71*, 2652–2661.

(55) Sato, T.; Akahane, T.; Amano, K.; Hyodo, R.; Yanase, K.; Ogura, T. Scattering and Spectroscopic Study on the Hydration and Phase Behavior of Aqueous Alcohol Ethoxylate and Methyl Ester Ethoxylate: Effects of Terminal Groups in Hydrophilic Chains. *J. Phys. Chem. B* **2016**, *120*, 5444–5454.

(56) Lide, D. R. *CRC Handbook of Chemistry and Physics, 85th Edition*; CRC Press: Boca Raton, 2004.

(57) Okan, S. E.; Champeney, D. C. Molar Conductance of Aqueous Solutions of Sodium, Potassium, and Nickel Trifluoromethanesulfonate at 25 °C. *J. Solution Chem.* **1997**, *26*, 405–414.

(58) Bockris, J. O.; Reddy, A. K. N. *Modern Electrochemistry*, 2nd ed.; Plenum: New York, 1998; Vol. 1.

(59) Replacement of the present infinite-dilution diffusion coefficients by experimental $D(c)$ values does not improve the situation as diffusion coefficients of free ions generally depend only weakly on concentration.[58]

(60) Rehage, H.; Hoffmann, H. Rheological Properties of Viscoelastic Surfactant Systems. *J. Phys. Chem.* **1988**, *92*, 4712–4719.

(61) Kern, F.; Lequeux, F.; Zana, R.; Candau, S. J. Dynamic Properties of Salt-free Viscoelastic Micellar Solutions. *Langmuir* **1994**, *10*, 1714–1723.

(62) Naskar, B.; Diat, O.; Nardello-Rataj, V.; Bauduin, P. Nanometer-Size Polyoxometalate

Anions Adsorb Strongly on Neutral Soft Surfaces. *J. Phys. Chem. C* **2015**, *119*, 20985–20992.

(63) Bauer, C.; Bauduin, P.; Girard, L.; Diat, O.; Zemb, T. Hydration of sugar based surfactants under osmotic stress: A SAXS study. *Colloids and Surfaces A: Physicochemical and Engineering Aspects* **2012**, *413*, 92–100.

(64) Pedersen, J. S. Analysis of small-angle scattering data from colloids and polymer solutions: modeling and least-squares fitting. *Adv. Colloid Interface Sci.* **1997**, *70*, 171–210.

(65) Schulz, P. C. Steric Fitting of the Spherical Micelle Size. *Colloid Polym. Sci.* **1991**, *269*, 612–619.

(66) Kusano, T.; Fujii, K.; Tabata, M.; Shibayama, M. Small-Angle Neutron Scattering Study on Aggregation of 1-Alkyl-3-methylimidazolium Based Ionic Liquids in Aqueous Solution. *J. Solution Chem.* **2013**, *42*, 1888–1901.

(67) Brandes, E.; Stage, C.; Motschmann, H.; Rieder, J.; Buchner, R. Is Surface Layering of Aqueous Alkali Halides Determined by Ion Pairing in the Bulk Solution? *J. Chem. Phys.* **2014**, *141*, 18C509.

(68) Bešter-Rogač, M.; Stoppa, A.; Hunger, J.; Hefter, G.; Buchner, R. Association of Ionic Liquids in Solution: A Combined Dielectric and Conductivity Study of [bmim][Cl] in Water and in Acetonitrile. *Phys. Chem. Chem. Phys.* **2011**, *13*, 17588–17598.

(69) Migliorati, V.; Zitolo, A.; D'Angelo, P. Using a Combined Theoretical and Experimental Approach to Understand the Structure and Dynamics of Imidazolium-Based Ionic Liquids/Water Mixtures. 1. MD Simulations. *J. Phys. Chem. B* **2013**, *117*, 12505–12515.

(70) Spickermann, C.; Thar, J.; Lehmann, S. B. C.; Zahn, S.; Hunger, J.; Buchner, R.; Hunt, P. A.; Welton, T.; Kirchner, B. Why are Ionic Liquids Mainly Associated in

Water? A Car-Parinello Study of 1-Ethyl-3-methyl-imidazolium Chloride Water Mixture. *J. Chem. Phys.* **2008**, *129*, 104505.

(71) Halle, B.; Carlström, G. Hydration of Ionic Surfactant Micelles from Water Oxygen-17 Magnetic Relaxation. *J. Phys. Chem.* **1981**, *85*, 2142–2147.

(72) Pal, S.; Bagchi, B.; Balasubramanian, S. Hydration Layer of a Cationic Micelle, C_{10}TAB: Structure, Rigidity, Slow Reorientation, Hydrogen Bond Lifetime, and Solvation Dynamics. *J. Phys. Chem. B* **2005**, *109*, 12879–12890.

(73) Lima, F. S.; Chaimovich, H.; Cuccovia, I. M.; Horinek, D. Molecular Dynamics Shows That Ion Pairing and Counterion Anchoring Control the Properties of Trifalte Micelles: A Comparison with Triflate at the Air/Water Interface. *Langmuir* **2014**, *30*, 1239–1249.

(74) Bhargava, B. L.; Klein, M. L. Initial Stages of Aggregation in Aqueous Solutions of Ionic Liquids: Molecular Dynamics Studies. *J. Phys. Chem. B* **2009**, *113*, 9499–9505.

(75) Matthews, R. P.; Welton, T.; Hunt, P. A. Competitive pi Interactions and Hydrogen Bonding within Imidazolium Ionic Liquids. *Phys. Chem. Chem. Phys.* **2014**, *16*, 3238–3253.

(76) Li, X.-W.; Zhang, J.; Dong, B.; Zheng, L.-Q.; Tung, C.-H. Characterization of Lyotropic Liquid Crystals Formed in the Mixtures of 1-Alkyl-3-methylimidazolium Bromide/p-Xylene/Water. *Colloids Surf., A* **2009**, *335*, 80–87.

(77) Lima, F. S.; Cuccovia, I. M.; Horinek, D.; Amaral, L. Q.; Riske, K. A.; Schreier, S.; Salinas, R. K.; Bastos, E. L.; Pires, P. A. R.; Bozelli, J. C.; Favaro, D. C.; Rodrigues, A. C. B.; Dias, L. G.; El Seoud, O. A.; Chaimovich, H. Effect of Counterions on the Shape, Hydration, and Degree of Order at the Interface of Cationic Micelles: The Triflate Case. *Langmuir* **2013**, *29*, 4193–4203.

(78) Vanyur, R.; Biczok, L.; Miskolczy, Z. Micelle Formation of 1-Alkyl-3-methylimidazolium Bromide Ionic Liquids in Aqueous Solution. *Colloids Surf. A* **2007**, *299*, 256–261.

(79) Wang, J.; Wang, H.; Zhang, S.; Zhang, H.; Zhao, Y. Conductivities, Volumes, Fluorescence, and Aggregation Behavior of Ionic Liquids $[C_4mim][BF_4]$ and $[C_nmim]Br$ (n = 4, 6, 8, 10, 12) in Aqueous Solutions. *J. Chem. Phys. B* **2007**, *111*, 6181–6188.

(80) Stewart, J. J. *MOPAC 2012*; Stewart Computational Chemistry: Colorado Springs, CO, USA, 2012.

(81) In this calculation it was assumed that the apparent molar volumes of the ILs, calculated from the density values of Tables S1-S3, are equal to V_ϕ^{mic} as for $c > cmc$ the obtained data were constant within error limits.

(82) Lee, A. L.; Perez-Martinez, C. S.; Smith, A. M.; Perkin, S. Scaling Analysis of the Screening Length in Concentrated Electrolytes. *Phys. Rev. Lett.* **2017**, *119*, 026002.

(83) Hölzl, C. Optimierung einer TDR-Apparatur zur Untersuchung der dielektrischen Relaxationvon H_2O, D_2O und wässrigen Tetraalkylammoniumbromidlösungen. Ph.D. thesis, Regensburg University, 1998.

(84) Schrödle, S. Effects of Non-ionic Surfactants and Related Compounds on the Cooperative and Molecular Dynamics of their Aqueous Solutions. Ph.D. thesis, Regensburg University, 2005.

(85) Rønne, C.; Åstrand, P.-O.; Keiding, S. R. THz Spectroscopy of H_2O and D_2O. *Phys. Rev. Lett.* **1999**, *82*, 2888–2891.

(86) Ellison, W. J.; Lamkaouchi, K.; Moreau, J.-M. Water: A Dielectric Reference. *J. Mol. Liq.* **1996**, *68*, 171–279.

Graphical TOC Entry